

# Variational Monte Carlo (VMC) on a 3 dimensional model of *Hookium*, a two electron harmonium in a Hooke's potential, with parallelisation on a GPU

Blaž Stojanovič

Cavendish Laboratory, Department of Physics, JJ Thomson Avenue, Cambridge. CB3 0HE

---

## Abstract

REDO

In this written assignment, we implement a Variational Quantum Monte Carlo (VMC) code to study the three dimensional, two electron *Hookium* system. We calculate the ground state wavefunction in position space, and compare it to a known analytical solution, both directly and via position and via intracule. With aid from the Hartree-Fock method, we estimate the correlation energy of the system. The code is implemented in Python using the JAX library and is extended to work on graphical processing units (GPUs), a comparison between CPU and GPU performance is conducted.

---

## Contents

<b>1</b>	<b>Introduction</b>	<b>1</b>
1.1	Quantum Monte Carlo methods . . . . .	2
1.2	Graphical processing units . . . . .	3
1.3	Hookium . . . . .	3
<b>2</b>	<b>Implementation</b>	<b>4</b>
2.1	Monte Carlo Importance Sampling . . . . .	4
2.2	Metropolis-Hastings algorithm . . . . .	4
2.3	Variational Quantum Monte Carlo . . . . .	5
2.3.1	Trial wave functions $\Psi_T$ . . . . .	6
2.3.2	Basis sets . . . . .	6
2.3.3	Generating trial moves . . . . .	7
2.4	Technical Considerations . . . . .	7
2.4.1	Software structure . . . . .	7
2.4.2	Automatic differentiation . . . . .	7
2.4.3	Gradient estimators . . . . .	7
2.4.4	Parallelization . . . . .	7
2.4.5	GPU Acceleration . . . . .	7
<b>3</b>	<b>Results and analysis</b>	<b>8</b>
3.1	Hookium . . . . .	8
3.1.1	HF energy . . . . .	8
3.1.2	Variational Monte Carlo . . . . .	8
3.1.3	Variational Monte Carlo . . . . .	8
3.1.4	CPU vs. GPU speedup . . . . .	8
3.2	Hookium molecule . . . . .	8

<b>4</b>	<b>Conclusion</b>	<b>9</b>
4.1	Code expandability and complexity . . . . .	9

<b>Bibliography</b>	<b>9</b>	
<b>Appendix A</b>	<b>Hartree-Fock</b>	<b>11</b>
<b>Appendix B</b>	<b>Basis sets</b>	<b>11</b>
Appendix B.1	Gaussian basis set . . . . .	11
Appendix B.2	Harmonic Oscillator basis set . . . . .	13

## 1. Introduction

The Schrödinger equation underpins a large part of quantum chemistry and solid state physics. However, the quantum many-body problem, which amounts to solving the  $3N$ -dimensional Schrödinger equation is notoriously hard to solve. Ever since the postulation of the equation in 1925, great efforts have been made in solving the equation, both analytically and numerically. Perhaps most impactful was the development of various approximate methods to solve the many-body problem with the available computational resources. Hartree-Fock (HF) approaches [1, 2] solve an auxiliary system of independent electrons in a self-consistent field and assume that the wave function (for fermions) can be represented as a single Slater determinant. HF method does not include electron correlation, which makes it a good approximation only in systems where

correlation contributions are small. Post-Hartree-Fock methods, such as Coupled Cluster, Configuration interaction and Møller-Plesset theory include correlation by considering a linear combination of determinants, they can be extremely accurate but come at a high computational cost.

One of the most popular approaches used today is Density Functional Theory (DFT). It reformulates the many-body electron problem in terms of the 3-dimensional electron density  $n(\mathbf{r})$ , which is found by minimising the total energy functional  $E[n(\mathbf{r})]$  [3]. DFT provides an alternative line of thought to the truncated Hilbert space of single particle orbitals [4] and is used extensively for simulating large systems as linear scaling variants of DFT exist [5]. While DFT is theoretically exact the true energy functional  $E[n(\mathbf{r})]$  is not known and its parameterisations employ more accurate *ab initio* methods. One of which being Quantum Monte Carlo (QMC).

### 1.1. Quantum Monte Carlo methods

Quantum Monte Carlo is a class of methods that use statistical sampling to directly deal with high-dimensional integration that arises from working with the many-body wave function. QMC methods are among the most accurate achieving chemical accuracy for smaller systems [6], and can achieve any degree of statistical precision sought. Quantum Monte Carlo is also very versatile and can be applied at both zero and finite temperatures [7]. The most basic zero temperature QMC method is variational QMC (VMC). The method is composed of roughly two parts, firstly it directly evaluates the variational energy  $E_V = \langle \Psi_T | H | \Psi_T \rangle / \langle \Psi_T | \Psi_T \rangle$  of the system using Monte Carlo integration and a trial wave function  $\Psi_T$ . Secondly the parameters of the trial wave function are optimised such as to minimise the variational energy  $E_V$ , giving the method its name. The first application of VMC was to ground state  $^4\text{He}$  [8], it was later extended for studying many-body fermionic systems [9]. A way of obtaining excitation energies using VMC is to use a trial wave function that models an excited state of the system, if the trial wave function obeys a certain symmetry, the variational principle guarantees that this VMC energy calculation gives an upper bound on the lowest exact eigenstate of this symmetry. Furthermore, the method can be extended to study non-equilibrium properties of bosonic [10, 11], and fermionic [12] systems. The main advantage of VMC is its simplicity while the main drawback is that the accuracy is limited by the flexibility and form of the trial wave function [7]. As such VMC is usually

employed as a first step in more advanced QMC simulations.

Projector quantum Monte Carlo (PMC), is a class of QMC methods which are in essence nothing more than stochastic implementations of the power method to obtain the dominant eigenvector of a matrix or a kernel function [13]. Their distinct advantage over VMC is that they are not constrained by our parametrization of the trial wave function, as they can describe arbitrary probability distributions. The projector  $\hat{P}$  has to be chosen in such a way, that the ground state of the system becomes the dominant eigenvector, i.e.  $|\Psi_0\rangle = \lim_{n \rightarrow \infty} \hat{P}^n |\Psi_T\rangle$ . Different ways of achieving this, the space (real or orbital space) in which the walk is done and choosing either first or second quantization description, give rise to different flavours of PMC methods. Using an exponential projector  $\hat{P} = e^{\tau(E_T \mathbb{1} - \hat{H})}$  can be interpreted as propagation in imaginary time  $\tau \rightarrow it$  in turn transforming the Schrödinger equation into a diffusion equation, which is a continuous limit of the random walk and lends itself to stochastic integration [14]. Directly sampling from the exact Green function is known as Projector Green Function Monte Carlo (GFMC) method [15, 16]. A convenient approximation to GFMC is its short-time approximation which leads to one of the most popular QMC methods, diffusion Monte Carlo (DMC) [6, 14]. In this regime one can exploit analytical solutions to diffusion and rate problems to write an explicit form of the Green's function. Additionally, by using the Trotter-Suzuki formula time-step bias can be expressed and accounted for [7]. DMC is statistically implemented by using a population of walkers which either branch or die, the average over all walkers is calculated. Reptation quantum Monte Carlo [14] (RMC) is an alternative formulation which only uses a single walker, and instead of branching and dying the MC moves mutate the path of that single walker. The use of a guiding wave function for importance sampling greatly improves the statistical efficiency of PMC methods, the guiding wave function is usually obtained by means of VMC or some mean field calculation.

PMC method suffer from the *sign problem*, which is present in Markov chain simulation of distributions that are not strictly positive, this is the case in fermionic and frustrated systems [13]. The problem refers to an exponential decrease in sampling efficiency with system size. The search for solutions of this problem is still an area of active research [6] but is in practice remedied by the *fixed-node* approximation [17]. In it a boundary condition is imposed into the projection, such that the

projected state shares the same zero crossings (nodal surface) with a trial wave function, which is again usually obtained with VMC. The projected state is now only exact when the nodal surface is exact, nevertheless this approximation is quite accurate [6]. Fixed node is widely used, one of its first applications was to the electron gas [18], which is used in parameterizations of the exchange correlation functional in LSDA [19].

Quantum Monte Carlo methods have had a lot of success at finite temperatures. Auxiliary-field Monte Carlo, or Path Integral Monte Carlo [20], which leads to ring-polymer molecular dynamics, may be used for this purpose. Additionally QMC is not limited to continuum space applications and has been extensively used to study lattice models, notable examples being the cluster/loop algorithm and the worm algorithm [13, 21].

Quantum Monte Carlo methods are generally more computationally expensive than DFT approaches, but on the other hand QMC codes are, as a rule of thumb, simpler to implement. Furthermore, since the wave function does not need to be stored directly QMC has reasonable storage requirements. The high computational cost of the QMC methods is remedied by the fact that they are intrinsically parallelisable, the core calculation involves generating (pseudo)-random numbers, performing a simple calculation and in the end averaging over the results. Therefore, implementations of QMC algorithms that have been applied to practical problems are optimised to run on massively parallel hardware with little overhead [22]. Finally, the repetitive nature of the Monte Carlo calculation lends itself to hardware acceleration using either graphical processing units (GPUs) or field-programmable gate arrays (FPGAs) [7].

### 1.2. Graphical processing units

Building customised hardware for graphics is common practice since the 1970s, but the term *graphical processing unit* (GPU) as we know it today was popularised at the turn of the millennium by NVIDIA. GPUs were originally designed with very specialised tasks in mind, but in the last two decades there has been an increased interest in leveraging GPU for various computationally intensive applications, usually referred to as *general-purpose computing on graphical processing units* (GPGPU). The main advantage of graphical processing units over CPUs is higher theoretical *floating point operations per second* (FLOPS) and increased theoretical bandwidth. This is achieved by dedicating a larger proportion of transistors in the processing unit to data processing as opposed to flow control

and data catching, as well as not performing branch checking [23], see Figure 1. GPUs were designed to

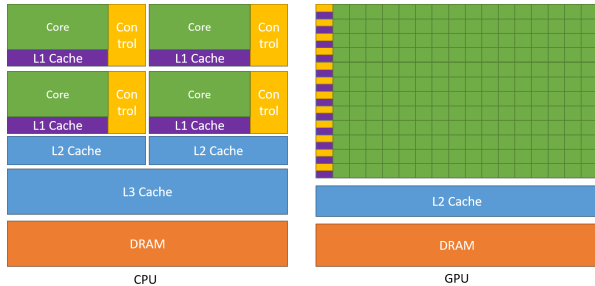


Figure 1: A comparison of a CPU and GPU, from [23].

work with small fragments of data (pixels) and perform the same operation many times simultaneously on all of the fragments. In the CUDA parallel programming model the problem at hand is required to be decomposed into tasks that can be independently executed in parallel by *blocks of threads*. The tasks must be such that they can be executed in parallel by the threads within a block. Each thread executes functions called *kernels*. A substantial speedup of a calculation can be achieved *if* it can be made to comply with the data and thread parallelism required for the above described procedure.

QMC methods can be made to fit this mold and there has been extensive work done in this direction [24, 25, 26]. GPUs can be exploited by initializing multiple walkers and running them in parallel thread blocks before averaging the results over all of them. Additionally GPUs can be used to accelerate the evaluation of basis function expansions, the linear algebra associated with computing the Slater determinant and evaluation of complicated forms of the Jastrow factor in Variational Monte Carlo. Since most GPUs only support single precision arithmetic, accuracy was of concern in first applications to QMC, benchmarks have shown that chemical accuracy is still achievable on GPUs [17, 25].

### 1.3. Hookium

We can construct a toy model of two electrons, that resembles the helium atom, where the electrons are bound to the nucleus with a harmonic instead of a Coulomb potential. The Hamiltonian of the model is then defined as

$$\hat{H} = -\frac{1}{2}\nabla_1^2 - \frac{1}{2}\nabla_2^2 + \frac{1}{2}kr_1^2 + \frac{1}{2}kr_2^2 + \frac{1}{r_{12}}. \quad (1)$$

This model is referred to as *hookium* (sometimes harmonium). Although it is quantitatively different from

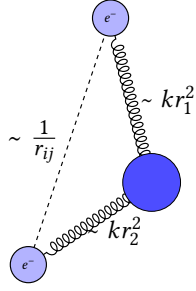


Figure 2: Hookium atom, two electrons that are bound to the nucleus with springs of coefficient  $k$  and interact via the Coulomb force.

helium some meaningful qualitative comparisons can be made [27]. Most notably hookium has an analytical solution for the case  $k = \frac{1}{4}$ , making it an ideal candidate to benchmark computational methods, which is the topic of this written assignment. The normalized closed form wave function solution of the ground state in position space is

$$\Psi(\mathbf{r}_1, \mathbf{r}_2) = \frac{1}{2\sqrt{8\pi^{5/2} + 5\pi^3}} \left(1 + \frac{r_{12}}{2}\right) \exp\left(-\frac{r_1^2 + r_2^2}{4}\right), \quad (2)$$

the energy of the state is  $E = 2$ . The probability of finding two electrons distance  $u$  apart is the position intractable  $P(u)$ , is also useful. It is defined as

$$P(u) = \iiint |\Psi(\mathbf{r}_1, \mathbf{r}_2)|^2 \delta(\mathbf{r}_{12} - \mathbf{u}) d\mathbf{r}_1 d\mathbf{r}_2 d\Omega_{\mathbf{u}}, \quad (3)$$

for hookium it too has a closed form

$$P(u) = \frac{1}{8 + 5\pi^{1/2}} u^2 \left(1 + \frac{u}{2}\right)^2 \exp\left(-\frac{u^2}{4}\right). \quad (4)$$

Values of  $h = m = c = 1$  and  $1E_h = 1$  will be assumed throughout this report. Hookium will be studied with the VMC method and the above expressions will be used to compare the accuracy of the numerical method.

The rest of this written assignment is structured as follows. In section 2, the details necessary to implement the variational Monte Carlo method are presented. Additionally details of GPU acceleration and parallelisation of the method are discussed. Presentation of numerical results and benchmarks of the method follow in section 3. The final section 4 contains a short conclusion and proposals for further work.

## 2. Implementation

### 2.1. Monte Carlo Importance Sampling

The most common application of Monte Carlo methods is evaluation of integrals in high dimensional space.

There MC has a distinct advantage over quadrature methods, as the statistical error decreases with the square root of samples regardless of the dimensionality of the problem. Integrals of a function  $g(\mathbf{R})$

$$I = \int g(\mathbf{R}) d\mathbf{R}, \quad (5)$$

where  $\mathbf{R}$  is the *configuration* of the system or simply a *walker*, can be integrated by use of an *importance function*  $P(\mathbf{R})$ , where  $\int d\mathbf{R} P(\mathbf{R}) = 1$  and  $P(\mathbf{R}) \geq 0$ . The integral can be rewritten in the form

$$\int g(\mathbf{R}) d\mathbf{R} = \int \frac{g(\mathbf{R})}{P(\mathbf{R})} P(\mathbf{R}) d\mathbf{R} = \int f(\mathbf{R}) P(\mathbf{R}) d\mathbf{R}, \quad (6)$$

where  $f(\mathbf{R}) = g(\mathbf{R})/P(\mathbf{R})$ . The importance function  $P(\mathbf{R})$  can be interpreted as a probability density. If we now generate an infinite number of random uncorrelated configurations  $\mathbf{R}_m$  from the distribution  $P(\mathbf{R})$ , the sample average is a good estimator of the integral  $I$

$$I = \lim_{M \rightarrow \infty} \left\{ \frac{1}{M} \sum_{m=1}^M f(\mathbf{R}_m) \right\}, \quad (7)$$

and for an approximation with a finite number of samples

$$I \approx \frac{1}{M} \sum_{m=1}^M f(\mathbf{R}_m). \quad (8)$$

Under conditions where the central limit theorem holds [6], the estimator is normally distributed with variance  $\sigma_f^2/M$ , which can also be estimated from the samples as

$$\frac{\sigma_f^2}{M} \approx \frac{1}{M(M-1)} \sum_{m=1}^M \left[ f(\mathbf{R}_m) - \frac{1}{M} \sum_{n=1}^M f(\mathbf{R}_n) \right]^2. \quad (9)$$

In the case of hookium the configurations  $\mathbf{R}$  are the positions of the electrons.

### 2.2. Metropolis-Hastings algorithm

The integration technique from the previous section relies on our ability to obtain samples from a probability distribution  $P(\mathbf{R})$ . In the case of QMC these distributions are high-dimensional and cannot be directly sampled from, moreover their normalizations are usually not known. The Metropolis-Hastings algorithm [28], see Algorithm 1, avoids direct sampling from the distribution  $P(\mathbf{R})$  and is insensitive to its normalization. It uses a Markov process whose stationary distribution  $\pi(\mathbf{R})$  is  $\pi(\mathbf{R}) = P(\mathbf{R})$  to generate a sequence of configurations  $\{\mathbf{R}_n\}_P$  that are drawn from  $P(\mathbf{R})$ . A Markov

process is completely defined with its transition probability  $P(\mathbf{R} \rightarrow \mathbf{R}')$ , which is the probability of transitioning from state  $\mathbf{R}$  to state  $\mathbf{R}'$ . For the process to have a unique stationary distribution two conditions must be met, the process must be *ergodic* and it must obey *detailed balance*

$$P(\mathbf{R})P(\mathbf{R} \rightarrow \mathbf{R}') = P(\mathbf{R}')P(\mathbf{R}' \rightarrow \mathbf{R}), \quad (10)$$

rewritten as

$$\frac{P(\mathbf{R})}{P(\mathbf{R}')} = \frac{P(\mathbf{R}' \rightarrow \mathbf{R})}{P(\mathbf{R} \rightarrow \mathbf{R}')}. \quad (11)$$

The right transition probability  $P(\mathbf{R} \rightarrow \mathbf{R}')$  is not known, but we can express it with a trial move transition probability  $T(\mathbf{R} \rightarrow \mathbf{R}')$  which we can sample and acceptance probability  $A(\mathbf{R} \rightarrow \mathbf{R}')$  as

$$P(\mathbf{R} \rightarrow \mathbf{R}') = T(\mathbf{R} \rightarrow \mathbf{R}')A(\mathbf{R} \rightarrow \mathbf{R}'). \quad (12)$$

For equation (11) to hold, the acceptance probability must be

$$A(\mathbf{R} \rightarrow \mathbf{R}') = \min \left( 1, \frac{T(\mathbf{R}' \rightarrow \mathbf{R})P(\mathbf{R}')}{T(\mathbf{R} \rightarrow \mathbf{R}')P(\mathbf{R})} \right). \quad (13)$$

Thus to sample from any probability distribution we need only have the ability to calculate probabilities  $P(\mathbf{R})$  and to sample from a trial transition probability  $T(\mathbf{R} \rightarrow \mathbf{R}')$ . The efficiency of the algorithm depends on the amount of trial moves that we reject. All trial moves would be accepted if  $T(\mathbf{R} \rightarrow \mathbf{R}') = P(\mathbf{R}')$ , which would just mean sampling from  $P$  directly and is the very problem we are trying to solve with Metropolis-Hastings.

---

#### Algorithm 1: Metropolis-Hastings

---

**Result:** A set of configurations  $\{\mathbf{R}_n\}_P$  sampled from  $P$

Initialize walker at random configuration  $\mathbf{R}$ ;

**while** no. samples less than  $N$  **do**

Generate new configuration  $\mathbf{R}'$  with transition probability  $T(\mathbf{R} \rightarrow \mathbf{R}')$ ;  
Accept the move  $(\mathbf{R} \rightarrow \mathbf{R}')$  with probability  $A(\mathbf{R} \rightarrow \mathbf{R}') = \min \left( 1, \frac{T(\mathbf{R}' \rightarrow \mathbf{R})P(\mathbf{R}')}{T(\mathbf{R} \rightarrow \mathbf{R}')P(\mathbf{R})} \right)$ ;  
Append  $\mathbf{R}$  to the set of configurations;

**end**

---

### 2.3. Variational Quantum Monte Carlo

Variational quantum Monte Carlo uses a trial wave function  $\Psi_T$ , which is an approximation to the true

ground state wave function, to directly evaluate the expectation value of  $\hat{H}$ , which provides an upper bound on the ground state energy

$$E_V = \frac{\langle \Psi_T | H | \Psi_T \rangle}{\langle \Psi_T | \Psi_T \rangle} = \frac{\int \Psi_T^*(\mathbf{R}) \hat{H} \Psi_T(\mathbf{R}) d\mathbf{R}}{\int \Psi_T^*(\mathbf{R}) \Psi_T(\mathbf{R}) d\mathbf{R}} \geq E_0. \quad (14)$$

The expression for the variational energy  $E_V$  can be rewritten as

$$E_V = \frac{\int |\Psi_T(\mathbf{R})|^2 \left( \Psi_T(\mathbf{R})^{-1} \hat{H} \Psi_T(\mathbf{R}) \right) d\mathbf{R}}{\int |\Psi_T(\mathbf{R})|^2 d\mathbf{R}}. \quad (15)$$

The above integral is estimated by using Metropolis-Hastings to sample a set of configurations  $\{\mathbf{R}_n\}_P$  from the probability distribution given by the (normalized) trial wave function as  $P(\mathbf{R}) = |\Psi_T(\mathbf{R})|^2 d\mathbf{R}$  and averaging these *local*  $E_L$  contributions

$$E_V \approx \frac{1}{M} \sum_{m=1}^M E_L(\mathbf{R}_m), \quad (16)$$

where

$$E_L(\mathbf{R}) = \Psi_T(\mathbf{R})^{-1} \hat{H} \Psi_T(\mathbf{R}). \quad (17)$$

The procedure is analogous for any other calculation of expectation value. Trial moves may be chosen in a variety of ways depending on the system studied, in the case of hookium we will use a Gaussian distribution centered at the current position of the walker.

Estimation of the variational energy  $E_V$  is only one part of a variational Monte Carlo simulation. The second part is the variational optimization of the trial wave function. The trial wave function  $\Psi_T$  is parameterized with a set of variational parameters  $\{\alpha_k\}$ , historically the number of parameters was low due to high computational cost [6]. The optimal parameters for the system are found by minimizing the *cost function*. A straightforward choice of cost function is the variational energy  $E_V$  in eq. (15). Given that its value is bounded below due to the variational principle, eq (14), its minimization gives parameters  $\{\alpha_k\}$  that give the best energy estimate for given parameterization. An alternative is to minimize the variance of energy

$$\sigma_E^2(\{\alpha_k\}) = \frac{\int \Psi_T^2(\{\alpha_k\}) [E_L(\{\alpha_k\}) - E_V(\{\alpha_k\})]^2 d\mathbf{R}}{\int \Psi_T^2(\{\alpha_k\}) d\mathbf{R}}, \quad (18)$$

this minimizes the statistical error of VMC estimation of energy. Most practical calculations are done by minimizing energy variance [6]. Minimization of energy variance works because of the *zero-variance* property, which is exclusive for quantum expectation values. If

the trial wave function  $\Psi_T$  is an exact eigenfunction of the Hamiltonian

$$\hat{H}|\Psi_T\rangle = E_V|\Psi_T\rangle, \quad (19)$$

then the local energy  $E_L$ , a random variable, does not depend on the sampled configuration  $\mathbf{R}$

$$E_L(\mathbf{R}) = \Psi_T(\mathbf{R})^{-1} \hat{H} \Psi_T(\mathbf{R}) = \Psi_T(\mathbf{R})^{-1} E_V \Psi_T(\mathbf{R}) = E_V, \quad (20)$$

is constant and hence has zero variance. This equality holds only when  $\Psi_T$  is an exact eigenfunction of the Hamiltonian. However, zero-variance property has important consequences for numerical stability of optimization, it means that energy variance minima are robust to finite sampling. Minimizing the variance of energy drives the trial wave function towards eigenstates of the Hamiltonian. Moreover, the statistical error associated with estimation of any expectation value  $\langle \hat{O} \rangle$  is proportional to the variance of  $\hat{O}$ , one can use the zero-variance condition to define a renormalized observable  $\tilde{O}$  with the same average and smaller variance [29] for more efficient sampling.

Various approaches to minimize the cost function can be taken, the simplest is trial and error using simple fitting procedures, this only works for small numbers of parameters. Alternatively a reweighting technique can be used to evaluate the energy or energy variance of a wave function with slightly different parameters  $\Psi_T(\{\alpha + \delta\alpha\})$  to the one already evaluated  $\Psi_T(\{\alpha\})$  [30], this increases the number of variational parameters that can be treated in small systems. Another option is to evaluate energy derivatives and use some sort of stochastic optimization technique, *stochastic gradient descent* being the simplest and *stochastic reconfiguration* [31] being a more elaborate alternative.

### 2.3.1. Trial wave functions $\Psi_T$

The choice of trial wave function  $\Psi_T$  is the limiting factor for the performance of VMC, it determines its statistical efficiency and its final accuracy. The choice of trial wave function flexible but must satisfy the following conditions [6]; both the wave function and its gradient must be finite where the potential is finite, the wave function must have the appropriate symmetry and integrals

$$\int \Psi_T^* \Psi_T, \quad \int \Psi_T^* \hat{H} \Psi_T \quad \text{and} \quad \int \Psi_T^* \hat{H}^2 \Psi_T \quad (21)$$

must exist. A popular choice and the one we will use in this project is the *Slater-Jastrow* state. The trial wave

function is a product of a Slater determinant  $D(\mathbf{R})$  of single particle states  $\{\psi_k(\mathbf{r})\}$

$$D(\mathbf{X}) = \frac{1}{\sqrt{N!}} \begin{vmatrix} \psi_1(\mathbf{x}_1) & \psi_2(\mathbf{x}_1) & \cdots & \psi_N(\mathbf{x}_1) \\ \psi_1(\mathbf{x}_2) & \psi_2(\mathbf{x}_2) & \cdots & \psi_N(\mathbf{x}_2) \\ \vdots & \vdots & \ddots & \vdots \\ \psi_1(\mathbf{x}_N) & \psi_2(\mathbf{x}_N) & \cdots & \psi_N(\mathbf{x}_N) \end{vmatrix} \quad (22)$$

and the *Jastrow correlation factor*  $J(\mathbf{X})$

$$\Psi_{SJ}(\mathbf{X}) = e^{J(\mathbf{X})} D(\mathbf{X}), \quad (23)$$

where  $\mathbf{X}$  is a configuration that contains both the spin and position degrees of freedom  $\mathbf{x}_i = (\mathbf{r}_i, s_i)$ . The discriminant is usually decomposed into spin up and down components as

$$D(\mathbf{X}) = D^\uparrow(\mathbf{r}_1, \dots, \mathbf{r}_{N_\uparrow}) D^\downarrow(\mathbf{r}_{N_\uparrow+1}, \dots, \mathbf{r}_N), \quad (24)$$

this is computationally beneficial as it results in smaller determinants and no explicit sum over spin. The Jastrow factor is heuristically constructed to incorporate electron correlation into the wave function. In most practical calculations it is limited to one- and two-body terms [6]

$$J(\mathbf{R}) = \underbrace{\sum_{i=1}^N \chi(\mathbf{r}_i)}_{\text{one-body}} - \frac{1}{2} \underbrace{\sum_{i=1}^N \sum_{j < i}^N u(\mathbf{r}_i, \mathbf{r}_j)}_{\text{two-body}}. \quad (25)$$

The first term describes the nuclear-electronic correlation and the second electron-electron correlation, in this project we will focus only on the second term. Various forms of  $u(\mathbf{r}_i, \mathbf{r}_j)$  exist depending on application area, a common form for atomic and molecular calculations is

$$u(r_{ij}) = \frac{a_{ij} r_{ij}}{1 + b_{ij} r_{ij}}. \text{TODOADVANCEDJASTROW} \quad (26)$$

The parameters  $a_{ij}$  are chosen to satisfy the *cusp conditions*,

$$\left. \frac{du}{dr} \right|_{r=0} = \begin{cases} \frac{1}{2}, & \text{for opposite spins,} \\ \frac{1}{4}, & \text{for parallel spins.} \end{cases} \quad (27)$$

and the  $b$  parameters remain to be optimized variationally.

### 2.3.2. Basis sets

There are various choices of single particle states  $\{\psi_k(\mathbf{r})\}$  that compose the Slater determinant. They can be obtained from less expensive electronic structure methods, popular choices being LDA or HF, they

can be from a standard basis set, such as atomic orbitals, Gaussian or plane wave sets, or they can be designed for the particular case at hand. In this work, we will compare performance of HF orbitals obtained from Cartesian Gaussian-type orbitals (GTOs)

$$G_{ijk}(\mathbf{r}, \alpha, \mathbf{A}) = (x - x_A)^i (y - y_A)^j (z - z_A)^k e^{-\alpha r_A^2}, \quad (28)$$

and HF orbitals obtained from the harmonic oscillator basis set

$$\phi_k(r) = \frac{H_{2k-1}(r/\sqrt{2})}{2^k \sqrt{(2k-1)!} r/\sqrt{2}} \frac{\exp(-r^2/4)}{(2\pi)^{3/4}}. \quad (29)$$

Both basis sets and implementation of Hartree-Fock are discussed in more detail in Appendix B and Appendix A.

### 2.3.3. Generating trial moves

When proposing trial moves, we would like to minimize the correlation between subsequent states  $\mathbf{R}$  and  $\mathbf{R}'$  as well as maximize the acceptance probability  $A(\mathbf{R} \rightarrow \mathbf{R}')$ . Trial move probability determines both the size and average acceptance of the moves, practice we seek a compromise between both. First proposal probabilities were symmetric, meaning that the acceptance probability factors into

$$A(\mathbf{R} \rightarrow \mathbf{R}') = \min \left( 1, \frac{P(\mathbf{R}')}{P(\mathbf{R})} \right) = \min \left( 1, \frac{|\Psi(\mathbf{R}')|^2}{|\Psi(\mathbf{R})|^2} \right). \quad (30)$$

However it is beneficial to use information from the probability distribution to aid sampling. A common choice of non-symmetric trial move probability and the one we will use is

$$T(\mathbf{R} \rightarrow \mathbf{R}') = \frac{1}{(2\pi\tau)^{3N/2}} \exp \left( -\frac{(\mathbf{R}' - \mathbf{R} - \mathbf{v}(\mathbf{R})\tau)^2}{2\tau} \right), \quad (31)$$

where  $\tau$  is the time step and  $\mathbf{v}(\mathbf{R}) = \nabla \Psi(\mathbf{R})/\Psi(\mathbf{R})$  is the drift velocity, that drives the Markov random walk in the direction of increasing  $|\Psi(\mathbf{R})|$  [13].

## 2.4. Technical Considerations

You write this after the software is complete

### 2.4.1. Software structure

### 2.4.2. Automatic differentiation

### 2.4.3. Gradient estimators

### 2.4.4. Parallelization

### 2.4.5. GPU Acceleration

a

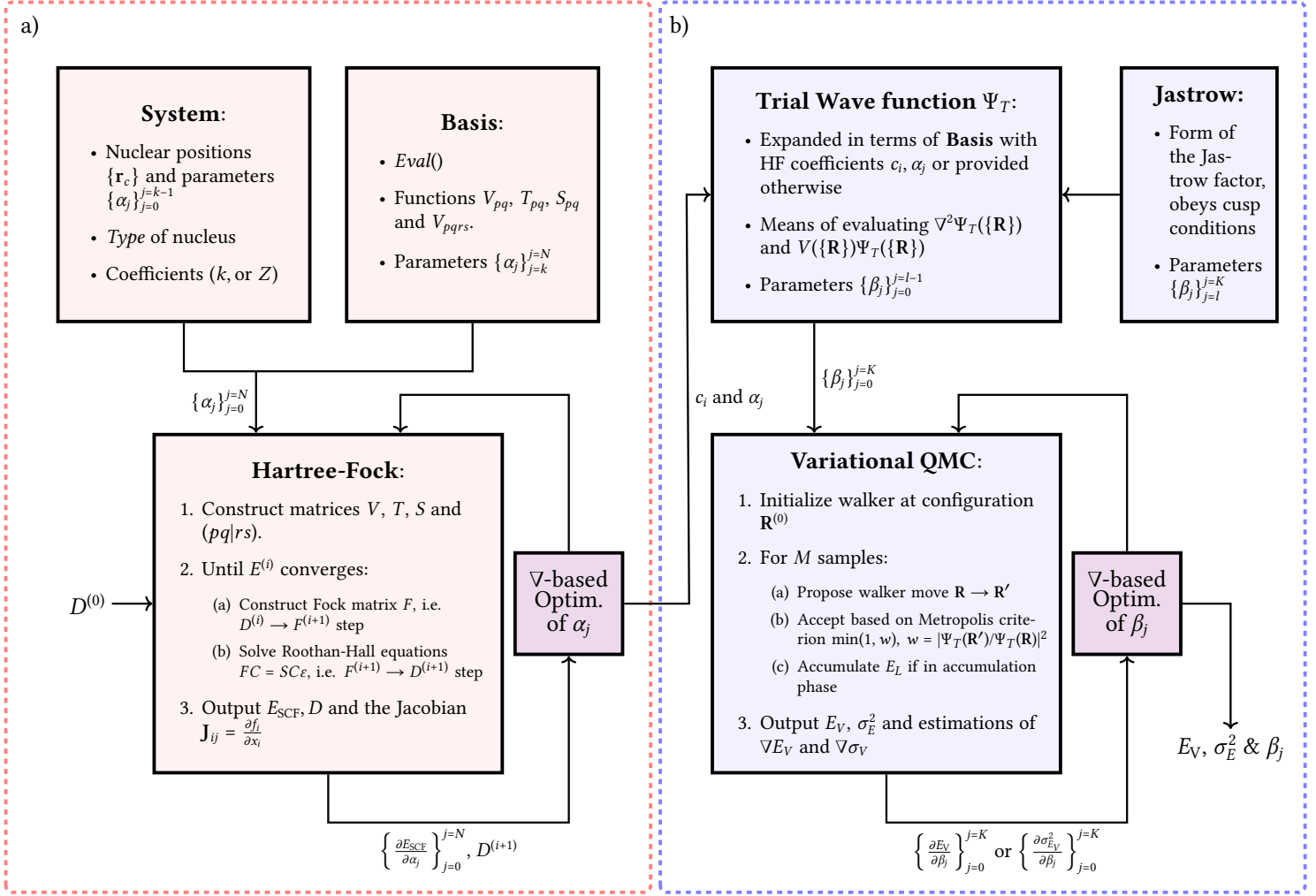


Figure 3: Diagram of the general software framework developed to solve the Hookium atom with VMC. It is comprised of two modules, that need not be used together. Both the a) Hartree-Fock and b) the VMC module are fully variational and allow for rich variational approaches to a particular problem.

b

### 3. Results and analysis

#### 3.1. Hookium

##### 3.1.1. HF energy

##### 3.1.2. Variational Monte Carlo

##### 3.1.3. Variational Monte Carlo

##### 3.1.4. CPU vs. GPU speedup

#### 3.2. Hookium molecule



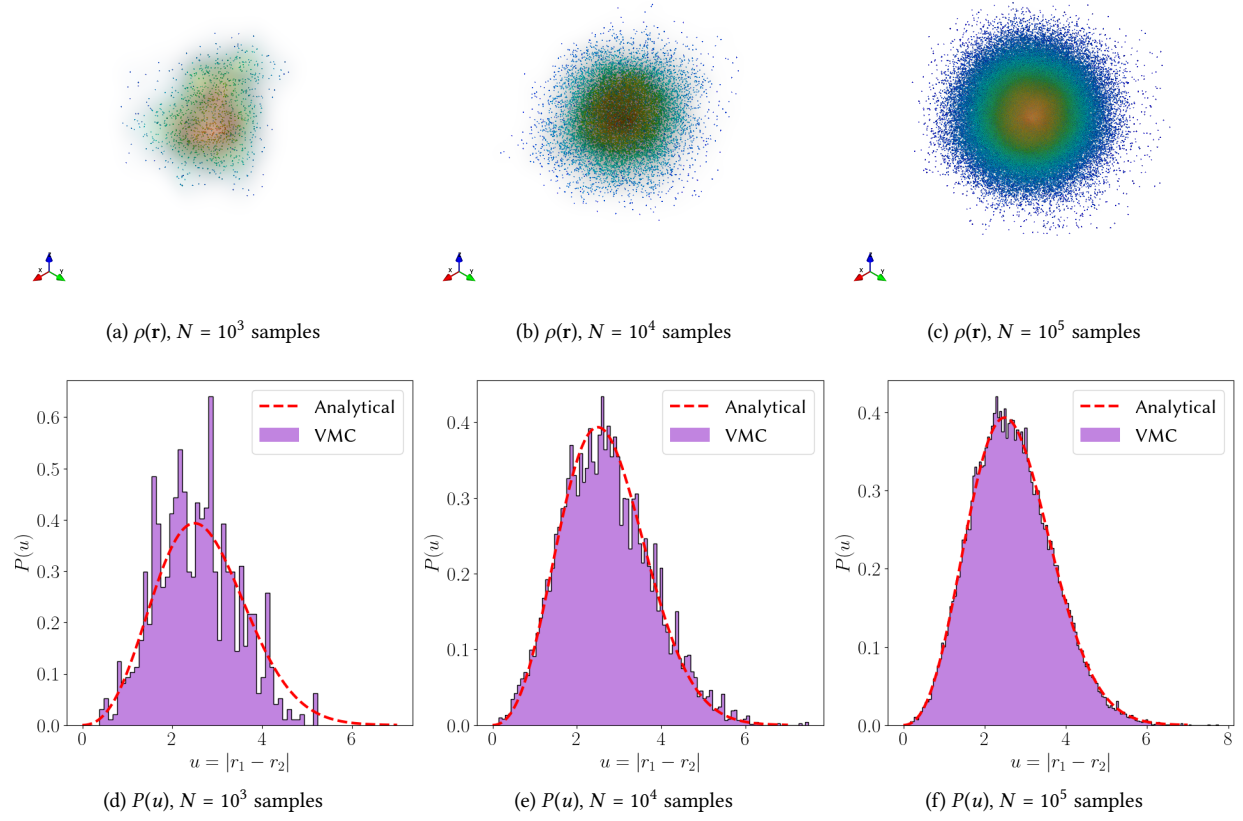


Figure 4: Blah blah results

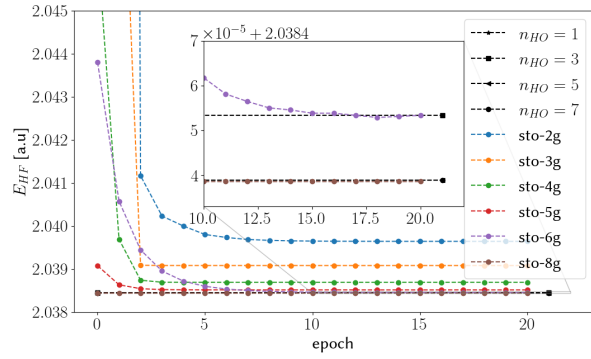


Figure 5

## 4. Conclusion

### 4.1. Code expandability and complexity

#### Bibliography

- [1] D. R. Hartree, The wave mechanics of an atom with a non-coulomb central field. part i. theory and methods, *Mathemat-*

- ical Proceedings of the Cambridge Philosophical Society 24 (1) (1928) 89–110. doi:10.1017/S0305004100011919.
- [2] V. Fock, Näherungsmethode zur lösung des quantenmechanischen mehrkörperproblems, *Zeitschrift für Physik* 61 (1-2) (1930) 126–148.
- [3] P. Hohenberg, W. Kohn, Inhomogeneous electron gas, *Physical review* 136 (3B) (1964) B864.
- [4] W. Kohn, Nobel lecture: Electronic structure of matter—wave functions and density functionals, *Reviews of Modern Physics* 71 (5) (1999) 1253.
- [5] C.-K. Skylaris, P. D. Haynes, A. A. Mostofi, M. C. Payne, Introducing onetep: Linear-scaling density functional simulations on parallel computers, *The Journal of chemical physics* 122 (8) (2005) 084119.
- [6] W. Foulkes, L. Mitas, R. Needs, G. Rajagopal, Quantum monte carlo simulations of solids, *Reviews of Modern Physics* 73 (1) (2001) 33.
- [7] B. M. Austin, D. Y. Zubarev, W. A. Lester Jr, Quantum monte carlo and related approaches, *Chemical reviews* 112 (1) (2012) 263–288.
- [8] W. L. McMillan, Ground state of liquid he 4, *Physical Review* 138 (2A) (1965) A442.
- [9] D. Ceperley, G. V. Chester, M. H. Kalos, Monte carlo simulation of a many-fermion study, *Physical Review B* 16 (7) (1977) 3081.
- [10] G. Carleo, F. Becca, M. Schiró, M. Fabrizio, Localization and

Basis	Optim.	$J_1$	$J_2$	$E_V \pm \sigma_E$
STO-2g + J1	✗	\	\	$2.375010 \pm 0.783208$
STO-4g + J1	✗	\	\	$2.024604 \pm 0.237808$
STO-2g + J1	✓	-0.06367405	\	$2.144614 \pm 0.508516$
STO-4g + J1	✓	0.32431903	\	$2.009259 \pm 0.169574$
1g + J1	✓	0.20198098	\	$2.000155 \pm 0.012942$
1g + J2	✓	0.22442447	-0.00406822	$2.000112 \pm 0.006640$

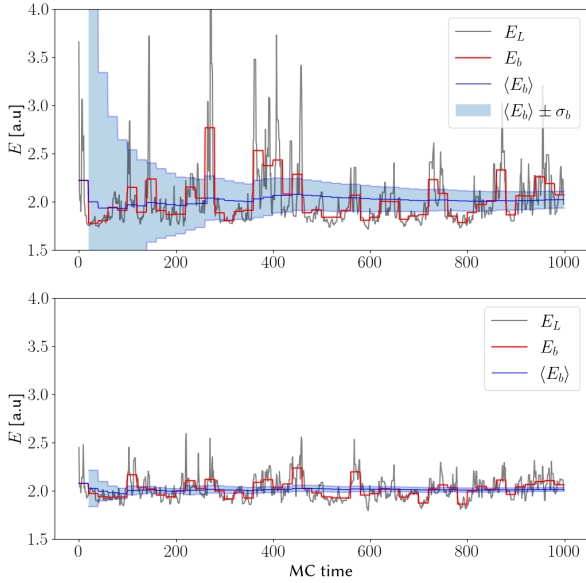


Figure 6

glassy dynamics of many-body quantum systems, Scientific reports 2 (1) (2012) 1–6.

- [11] G. Carleo, F. Becca, L. Sanchez-Palencia, S. Sorella, M. Fabrizio, Light-cone effect and supersonic correlations in one- and two-dimensional bosonic superfluids, *Physical Review A* 89 (3) (2014) 031602.
- [12] K. Ido, T. Ohgoe, M. Imada, Time-dependent many-variable variational monte carlo method for nonequilibrium strongly correlated electron systems, *Physical Review B* 92 (24) (2015) 245106.
- [13] J. Gubernatis, N. Kawashima, P. Werner, *Quantum Monte Carlo Methods: Algorithms for Lattice Models*, Cambridge University Press, 2016. doi:10.1017/CBO9780511902581.
- [14] P. J. Reynolds, J. Tobochnik, H. Gould, Diffusion quantum monte carlo, *Computers in Physics* 4 (6) (1990) 662–668.
- [15] M. Kalos, Monte carlo calculations of the ground state of three- and four-body nuclei, *Physical Review* 128 (4) (1962) 1791.
- [16] M. Kalos, Stochastic wave function for atomic helium, *Journal of Computational Physics* 1 (2) (1966) 257–276.
- [17] J. B. Anderson, A random-walk simulation of the schrödinger equation: H+ 3, *The Journal of Chemical Physics* 63 (4) (1975) 1499–1503.
- [18] D. M. Ceperley, B. J. Alder, Ground state of the electron gas by a stochastic method, *Physical review letters* 45 (7) (1980) 566.
- [19] S. H. Vosko, L. Wilk, M. Nusair, Accurate spin-dependent elec-

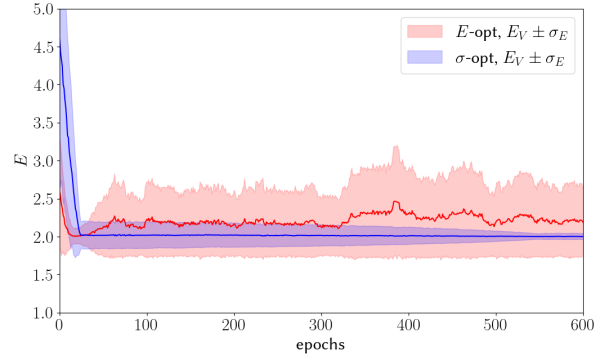


Figure 7

tron liquid correlation energies for local spin density calculations: a critical analysis, *Canadian Journal of physics* 58 (8) (1980) 1200–1211.

- [20] D. M. Ceperley, Path integrals in the theory of condensed helium, *Reviews of Modern Physics* 67 (2) (1995) 279.
- [21] N. Prokof'Ev, B. Svistunov, I. Tupitsyn, Exact, complete, and universal continuous-time worldline monte carlo approach to the statistics of discrete quantum systems, *Journal of Experimental and Theoretical Physics* 87 (2) (1998) 310–321.
- [22] R. Needs, M. Towler, N. Drummond, P. Lopez Rios, J. Trail, Variational and diffusion quantum monte carlo calculations with the casino code, *The Journal of chemical physics* 152 (15) (2020) 154106.
- [23] Cuda c++ programming guide, <https://docs.nvidia.com/cuda/cuda-c-programming-guide/index.html>.
- [24] A. G. Anderson, W. A. Goddard III, P. Schröder, Quantum monte carlo on graphical processing units, *Computer Physics Communications* 177 (3) (2007) 298–306.
- [25] J. S. Meredith, G. Alvarez, T. A. Maier, T. C. Schulthess, J. S. Vetter, Accuracy and performance of graphics processors: A quantum monte carlo application case study, *Parallel Computing* 35 (3) (2009) 151–163.
- [26] K. Esler, J. Kim, D. Ceperley, L. Shulenburger, Accelerating quantum monte carlo simulations of real materials on gpu clusters, *Computing in Science & Engineering* 14 (1) (2010) 40–51.
- [27] D. P. O'Neill, P. M. Gill, Wave functions and two-electron probability distributions of the hooke's-law atom and helium, *Physical Review A* 68 (2) (2003) 022505.
- [28] W. K. Hastings, Monte carlo sampling methods using markov chains and their applications (1970).
- [29] R. Assaraf, M. Caffarel, Zero-variance principle for monte carlo algorithms, *Physical review letters* 83 (23) (1999) 4682.
- [30] C. Umrigar, K. Wilson, J. Wilkins, Optimized trial wave func-

tions for quantum monte carlo calculations, Physical Review Letters 60 (17) (1988) 1719.

- [31] S. Sorella, Green function monte carlo with stochastic reconfiguration, Physical review letters 80 (20) (1998) 4558.
- [32] L. E. McMurchie, E. R. Davidson, One-and two-electron integrals over cartesian gaussian functions, Journal of Computational Physics 26 (2) (1978) 218–231.
- [33] S. Obara, A. Saika, Efficient recursive computation of molecular integrals over cartesian gaussian functions, The Journal of chemical physics 84 (7) (1986) 3963–3974.
- [34] J. T. Fermann, E. F. Valeev, Fundamentals of molecular integrals evaluation, arXiv preprint arXiv:2007.12057 (2020).
- [35] T. Helgaker, P. R. Taylor, Gaussian basis sets and molecular integrals, in: Modern Electronic Structure Theory: Part II, 1995, pp. 725–856.

## Appendix A. Hartree-Fock

Restricted Hartree-Fock is applicable to *closed-shell* systems, where there is an even number of electrons that form spin-up and spin-down pairs. The unrestricted Hartree-Fock calculation, where spin is explicitly considered, is only slightly more complicated. Both make use of a Slater determinant state and are solved using self-consistent field iteration. By far the most common approach is to expand single electron states in terms of a basis set, see Appendix B, as

$$\psi_i(\mathbf{r}) = \sum_{j=1}^n c_{ij} \phi_j(\mathbf{r}). \quad (\text{A.1})$$

An *exact* HF calculation gives an upper bound on the ground state energy of the system, this is because it does not contain electron correlation. In practice exact HF energy is not achieved because the basis set is finite. In the restricted case, truncated expansion in terms of a basis set leads to *Roothan-Hall equations*

$$\mathbf{FC} = \mathbf{SC}\epsilon. \quad (\text{A.2})$$

It is a nonlinear generalized eigenvalue problem, where the *Fock* matrix  $\mathbf{F}$  depends on the coefficient matrix  $\mathbf{C}$ .  $\mathbf{S}$  is the *overlap* matrix, essentially containing information of how close the basis set is to orthogonality

$$S_{pq} = \int \phi_p(\mathbf{r}) \phi_q(\mathbf{r}) d\mathbf{r}, \quad (\text{A.3})$$

and  $\epsilon$  is a diagonal matrix of orbital energies. The density matrix  $\mathbf{D}$  can be defined in terms of  $\mathbf{C}$  as

$$D_{pq} = 2 \sum_{a=1}^{\frac{N}{2}} c_{ap} c_{aq}, \quad (\text{A.4})$$

from which the electron density is easily expressed

$$\rho(\mathbf{r}) = \sum_{pq} D_{pq} \phi_p(\mathbf{r}) \phi_q(\mathbf{r}). \quad (\text{A.5})$$

The Fock matrix is in the literature usually decomposed into

$$\mathbf{F} = \mathbf{H}_{\text{core}} + \mathbf{G}, \quad (\text{A.6})$$

where  $\mathbf{H}_{\text{core}}$  is the sum of the kinetic and potential contributions

$$\mathbf{H}_{\text{core}} = \mathbf{T} + \mathbf{V}, \quad (\text{A.7})$$

defined in terms of basis functions as

$$T_{pq} = -\frac{1}{2} \int \phi_p(\mathbf{r}) \nabla^2 \phi_q(\mathbf{r}) d\mathbf{r} \quad (\text{A.8})$$

and

$$V_{pq} = \int \phi_p(\mathbf{r}) \left[ \sum_{A=1}^M V(\mathbf{r}, \{k_A\}) \right] \phi_q(\mathbf{r}) d\mathbf{r}. \quad (\text{A.9})$$

$\mathbf{G}$  is the two-electron contribution to the Fock operator, defined as

$$G_{pq} = \sum_{rs} D_{rs} \left[ (pq | rs) - \frac{1}{2} (pr | sq) \right] \quad (\text{A.10})$$

where  $(pq | rs)$  is the *two-electron* integral, in literature written in *chemists'* notation with round brackets

$$(pq | rs) = \int \frac{\phi_p(\mathbf{r}_1) \phi_q(\mathbf{r}_1) \phi_r(\mathbf{r}_2) \phi_s(\mathbf{r}_2)}{|\mathbf{r}_1 - \mathbf{r}_2|} d\mathbf{r}_1 d\mathbf{r}_2. \quad (\text{A.11})$$

In terms of quantities defined the energy of HF is

$$E = \text{Tr}(\mathbf{D}\mathbf{H}_{\text{core}}) + \frac{1}{2} \text{Tr}(\mathbf{D}\mathbf{G}). \quad (\text{A.12})$$

Roothan-Hall equations are solved by iterating between two steps. In the first step, the Fock matrix is constructed from the density matrix (i.e. expansion coefficients), and in the second a new set of coefficients and consequently a new density matrix is obtained by solving the generalized eigenvalue problem. Repeating the two steps converges the system towards self-consistency.

## Appendix B. Basis sets

### Appendix B.1. Gaussian basis set

Cartesian Gaussian-type orbitals (GTOs) are one of the most popular basis sets in computational chemistry. They were introduced as an approximation to Slater-type orbitals (STOs), as they massively simplify evaluations of integrals in from the previous section. Each Slater orbital is approximated by an expansion in Gaussian primitives centered at  $\mathbf{r}_A = (x_A, y_A, z_A)$ ,

$$G_{ijk}(\mathbf{r}, \alpha, \mathbf{A}) = (x - x_A)^i (y - y_A)^j (z - z_A)^k e^{-\alpha r_A^2}, \quad (\text{B.1})$$

where  $i, j, k$  combine into the total angular-momentum quantum number as  $l = i+j+k \geq 0$  and  $\alpha$  is a variational parameter, usually determined with some least-square fit to relevant Slater orbitals. Gaussians of a given total angular-momentum  $l$  form a shell, the  $s$ -shell is  $G_{000}$ ,  $p$ -shell are  $G_{100}$ ,  $G_{010}$  and  $G_{001}$ , and so on for  $d, f$ , etc. shells.

A large body of scientific work exists with regards to efficient evaluation of Gaussian-type orbital integrals arising from Hartree-Fock. Most approaches [32, 33] boil down to recursive relations that simplify the kinetic energy  $T_{pq}$  and two-electron ( $pq | rs$ ) integrals into overlap integrals  $S_{pq}$ . The most problematic integral is the nuclear-electron contribution which is not separable in Cartesian directions and requires special treatment. Even though the implementation of the general GTOs basis set is straightforward it proved to be too much work within the time constraints of this written assignment, it is thus a clear direction for expansion of the code in this work.

The integrals simplify considerably if we only consider a single site at  $\mathbf{r}_0 = (0, 0, 0)$ , which is enough to treat Hookium. The overlap integral  $S_{ijklmn}^{\alpha\beta} := S[G_{ijk}(\mathbf{r}, \alpha, 0), G_{lmn}(\mathbf{r}, \beta, 0)]$  decomposes into separate components along Cartesian axes  $S_{ijklmn}^{\alpha\beta} = S_{il}^{\alpha\beta} S_{jm}^{\alpha\beta} S_{kn}^{\alpha\beta}$  each with closed form solution

$$S_{il}^{\alpha\beta} = \int_{-\infty}^{\infty} x^{i+l} e^{-\alpha x^2 - \beta x^2} dx = \frac{1}{2} \left( 1 + (-1)^{i+l} \right) \sqrt{\frac{1}{(\alpha + \beta)^{1+i+j}}} \Gamma \left( \frac{1+i+l}{2} \right), \quad (\text{B.2})$$

where  $\Gamma$  is the gamma function. The integral vanishes for odd sums  $i+l$ . As in the general case, other integrals will be expressed in terms of overlap integrals for easier evaluation, starting with the nuclear attraction contribution  $V_{ijklmn}^{\alpha\beta} = V_{il}^{\alpha\beta} V_{jm}^{\alpha\beta} V_{kn}^{\alpha\beta}$ , for each Cartesian axis we get

$$V_{il}^{\alpha\beta} = k \int_{-\infty}^{\infty} x^i e^{-\alpha x^2} x^2 x^l e^{-\beta x^2} dx = k S_{i+2l}^{\alpha\beta} = k S_{il+2}^{\alpha\beta}. \quad (\text{B.3})$$

The kinetic energy matrix elements are simplified with use of the derivative identity

$$\frac{\partial}{\partial x} G_{ijk} = i G_{i-1jk} - 2\alpha G_{i+1jk}, \quad (\text{B.4})$$

consequently

$$\frac{\partial^2}{\partial x^2} G_{ijk} = 4\alpha^2 G_{i+2jk} - 2\alpha(2i+1)G_{ijk} + i(i-1)G_{i-2jk}. \quad (\text{B.5})$$

Again, Laplacian operator allows for decomposition into  $(xyz)$  components,  $T_{ijklmn}^{\alpha\beta} = T_{il}^{\alpha\beta} T_{jm}^{\alpha\beta} T_{kn}^{\alpha\beta}$  each contributing

$$T_{il}^{\alpha\beta} = -\frac{1}{2} \int_{-\infty}^{\infty} x^i e^{-\alpha x^2} \frac{\partial^2}{\partial x^2} \left( x^l e^{-\beta x^2} \right) dx, \quad (\text{B.6})$$

expressed with overlap integrals

$$T_{il}^{\alpha\beta} = -2\beta^2 S_{il+2}^{\alpha\beta} + \beta(2l+1)S_{il}^{\alpha\beta} - \frac{i}{2}(i-1)S_{il-2}^{\alpha\beta}. \quad (\text{B.7})$$

The two-electron integral is the most difficult, it cannot be expressed as a product of integrals for each axis. Closed form solutions for arbitrary angular momenta exist but include a 15-fold summation and are impractical for anything but  $(ss|ss)$  integrals. In practice the expression is evaluated by using a recursive relation to break down high angular momentum integrals into only  $(ss|ss)$ -type contributions [34]. We use the Obara-Saika scheme, following notation from notation from [35]. First we recursively define Hermite Gaussians  $E_t^{ij}$  as

$$\begin{aligned} E_t^{ij} &= \frac{1}{2p} E_{t-1}^{i,j-1} + \frac{qQ_x}{\beta} E_t^{i,j-1} + (t+1)E_{t+1}^{i,j-1} \\ E_t^{ij} &= \frac{1}{2p} E_{t-1}^{i-1,j} - \frac{qQ_x}{\alpha} E_t^{i-1,j} + (t+1)E_{t+1}^{i-1,j} \end{aligned} \quad (\text{B.8})$$

$$E_0^{00} = K_{AB}$$

$$E_t^{ij} = 0 \quad \text{if} \quad t < 0, \quad \text{or} \quad t > i+j,$$

where the auxiliary variables  $K_{AB}$ ,  $Q_x$ ,  $q$ ,  $p$  and  $P_x$  are defined for two Gaussians with  $\alpha$  and  $\beta$  at positions  $\mathbf{r}_A, \mathbf{r}_B$  as

$$\begin{aligned} K_{AB} &= \exp(-qQ_x^2) \\ Q_x &= x_A - x_B \\ q &= \frac{\alpha\beta}{\alpha + \beta} \\ p &= \alpha + \beta \\ P_x &= \frac{1}{p} (\alpha x_A + \beta x_B). \end{aligned} \quad (\text{B.9})$$

For our simplified case of coinciding only first terms in the recurrence relation (B.8) are nonzero and  $K_{AB} = 1$ . Additionally we need to define the auxiliary Hermite Coulomb integral  $R_{tuv}^n(p, \mathbf{r}_P, \mathbf{R}_C)$  between Gaussian at  $\mathbf{r}_P$  and Coulomb charge center at  $\mathbf{R}_C$  as

$$\begin{aligned} R_{t+1,u,v}^n &= t R_{t-1,u,v}^{n+1} + (x_P - x_C) R_{t,u,v}^{n+1} \\ R_{t,u+1,v}^n &= u R_{t,u-1,v}^{n+1} + (y_P - y_C) R_{t,u,v}^{n+1} \\ R_{t,u,v+1}^n &= v R_{t,u,v-1}^{n+1} + (z_P - z_C) R_{t,u,v}^{n+1} \\ R_{0,0,0}^n &= (-2p)^n F_n(p R_{PC}^2). \end{aligned} \quad (\text{B.10})$$

Again the relations simplify for our case,  $F_n$  is the Boys function, a special case of the incomplete Gamma function

$$F_n(x) = \int_0^1 \exp(-xt^2) t^{2n} dt. \quad (\text{B.11})$$

The two-body integral  $(pq|rs)$  is evaluated as [35]

$$(pq|rs) = \frac{2\pi^{5/2}}{pp' \sqrt{p+p'}} \sum_{tuv} E_{tuv}^{ab} \sum_{t'u'v'} (-1)^{t'+u'+v'} \times E_{t'u'v'}^{cd} R_{t+t', u+u', v+v'}(\alpha, \mathbf{P}, \mathbf{P}'), \quad (\text{B.12})$$

where  $p = \alpha + \beta$  and  $p' = \gamma + \delta$  are sums of Gaussian exponents.

#### Appendix B.2. Harmonic Oscillator basis set

The harmonic Oscillator basis set is composed of eigenfunctions of the Harmonic oscillator in three dimensions

$$\phi_k(r) = \frac{H_{2k-1}(r/\sqrt{2})}{2^k \sqrt{(2k-1)!} \sqrt{2}} \frac{\exp(-r^2/4)}{(2\pi)^{3/4}}. \quad (\text{B.13})$$

This basis set is not nearly as commonly used as the GTOs, but is a good enough basis set for Hooke's law atom. The integrals required for Hartree-Fock are straightforward to compute and cheap to evaluate, especially with no angular dependence involved, one only needs to use Hermite recurrence relations

$$H_{n+1}(x) = 2xH_n(x) - H'_n(x), \quad (\text{B.14})$$

where the derivatives satisfy

$$H'_n(x) = 2nH_{n-1}(x). \quad (\text{B.15})$$

The overlap integral is the most straightforward, using orthogonality between the polynomials

$$\int_{-\infty}^{\infty} H_m(x) H_n(x) e^{-x^2} dx = \sqrt{\pi} 2^n n! \delta_{nm}, \quad (\text{B.16})$$

we obtain

$$S_{kl} = \int_0^{\infty} \phi_k(r) \phi_l(r) 4\pi r^2 dr = \delta_{kl}. \quad (\text{B.17})$$

The potential matrix element is not much more difficult to compute

$$\begin{aligned} V_{kl} &= k \int_0^{\infty} \phi_k(r) r^2 \phi_l(r) 4\pi r^2 dr = \\ &= (4k-1)\delta_{kl} + \delta_{kl+1} \sqrt{4k^2 - 6k + 2} \\ &\quad + \delta_{kl-1} \sqrt{4k^2 + 2k}, \end{aligned} \quad (\text{B.18})$$

because one uses the recurrence relations once  $V_{kl}$  is tridiagonal instead of diagonal. The kinetic integral is a bit more arduous to evaluate and involves several applications of aforementioned recurrence and derivative expressions

$$\begin{aligned} T_{kl} &= -\frac{1}{2} \int_0^{\infty} \phi_k(r) (\nabla^2 \phi_l(r)) 4\pi r^2 dr = \\ &= \frac{(3+4k)}{8} \delta_{kl} - \frac{1}{4} \delta_{kl+1} \sqrt{\frac{1}{2}(1-3n+2n^2)} \\ &\quad - \frac{1}{4} \delta_{kl-1} \sqrt{\frac{1}{2}(n+2n^2)}. \end{aligned} \quad (\text{B.19})$$

The two-electron integral is the toughest to perform, depending on the type of basis function it is solved by using either a multipole expansion for the  $\propto \frac{1}{r_{12}}$  term, representing the term using a Laplace transform, or performing the integral in Fourier space. The latter approach works in the case of harmonic-oscillator basis, because the Fourier transform of a product of two basis functions  $\phi_k, \phi_j$  is an even polynomial multiplied by an exponential factor.